Noncovalent Interactions Between Molecular Hydrogen and the Alkali Fluorides: H-H···F-M (M = Li, Na, K, Rb, Cs). High Level Theoretical Predictions and SAPT Analysis.

Dan Zhou,[a] Guoliang Li,*[a,b,c] Kevin B. Moore III,[c] Yaoming Xie,[c] Kirk A. Peterson,[d] and Henry F. Schaefer III*[c]

[a]MOE Key Laboratory of Theoretical Chemistry of the Environment, Center for Computational Quantum Chemistry, South China Normal University, Guangzhou 510006, China
[b]Guangzhou Key Laboratory of Materials for Energy Conversion and Storage, School of Chemistry and Environment, South China Normal University, Guangzhou 510006, China
[c]Center for Computational Quantum Chemistry, University of Georgia, Athens, GA 30602, USA
[d]Department of Chemistry, Washington State University, Pullman, WA 99164-4630, USA
e-mails: ccq@uga.edu and glli@scnu.edu.cn

ABSTRACT:

Various types of hydrogen bonds have been recognized during the past century. In this research, a new type of noncovalent interaction, the dipole-induced hydrogen bond formed between a hydrogen molecule and an alkali halide, H-H···F-M, is studied. Proposed by Zhang and coworkers (*Phys. Chem. Chem. Phys.* 2015, **17**, 20361), these systems are extensively investigated initially using the "gold standard" CCSD(T) method in conjunction with augmented correlation-consistent polarized core-valence basis sets up to quadruple zeta. The full triple excitations CCSDT method has been used to further refine the energies. Several properties including geometries, bond energies, vibrarional frequencies, charge distributions, and dipole moments have been reported. The earlier Zhang research considered only the linear H-H···F-M structures. However, we find these linear stationary points to be separated by very small barriers from the much lower lying bent C_s structures. The CCSDT/aug-cc-pCVQZ(-PP) method predicts the dissociation energies for bent H-H···F-M (M = Li, Na, K, Rb, Cs) are 2.76, 2.96, 3.00, 2.89, and 2.49 kcal mol^{-1}, respectively, suggesting that the H···F hydrogen bond becomes gradually stronger when alkali metal M goes down the periodic table from Li to K, but becomes slightly weaker for Rb and even more for Cs. This Li < Na < K > Rb > Cs order is consistent with that for the dipole moments for the isolated MF (M = Li, Na, K, Rb, Cs) diatomics. Symmetry adapted perturbation theory (SAPT) is used to understand these unusual noncovalent interactions.

1. Introduction

Hydrogen bonds (HBs) play an important role in many physical, chemical, and biochemical processes,[1,2,3] which make them of very general concern. The HB is typically an attractive interaction between two polar groups: 1) the proton donor, a hydrogen atom covalently bound to a highly electronegative atom, and 2) the proton acceptor, another nearby highly electronegative atom. In 1939 Pauling[4] depicted HBs as X-H···Y, where X and Y (such as N, O, and F) are electronegative atoms, X-H with a typical polar covalent bond is the proton donor, and Y is the proton acceptor.

As time passed, the concept of the HB has evolved,[5] and some new types of HBs are being recognized. These include those containing nontraditional proton donor C-H units,[6,7] those with nontraditional proton acceptors (carbon atoms; π-electronic units; or even transition metal atoms);[8,9,10,11] and those with both nontraditional proton donors and nontraditional proton acceptors.[12,13,14,15,16] Finally, we might note dihydrogen bonds C-H···H-C, X-H···H-Si or X-H···H-M, where M is a metal atom, X-H is the typical proton donor, and the other hydrogen atom, H(M), with an excess of electron density, is the proton acceptor.[17,18,19,20,21,22] Very recently, Weinhold et al. have proposed the "anti-electrostatic" hydrogen bond (AEHB), formed between closed-shell ions of like charge.[23,24,25,26] This new concept may help to further reveal the nature of hydrogen bonds.

Beginning in 2000, hydrogen bonds were found between the H_2 molecule and the halide anions,[27,28,29] and in such system the H_2 subunit is largely maintained in the complex. The polar $M^{\delta+}-X^{\delta-}$ (metal-halogen) molecule was found to be a good

HB-acceptor.[30]   Zhang *et al.* recently described a new class of noncovalent interactions, H-H···Y-M (Y = F, Cl, Br; M = Li, Na, K, excluding Rb and Cs), and proposed that one can use a metal decorating method to increase the HB energy.[31]   In the present research, extensive *ab initio* investigations were carried out on the H-H···F-M (M = Li, Na, K, Rb, Cs) systems, using coupled-cluster methods with the basis sets up to aug-cc-pCVQZ, to provide this type of hydrogen bonding with definitive predictions.   Symmetry adapted perturbation theory (SAPT) is used to understand the electronic structures of H-H···F-M systems.

2. Computational Details

In this research, the H-H···F-M (M = Li, Na, K, Rb, Cs) systems were fully optimized and characterized by harmonic vibrational frequency analyses using the CCSD(T) method, which denotes the coupled cluster single- and double-substitution method with a perturbative treatment of triple excitations.[32,33,34]   To obtain yet more reliable energetics, single point energies were computed with the CCSDT method, which stands for the coupled cluster single-, double- and full triple-substitution method,[35,36] which is one of the most reliable among convergent quantum mechanical methods.

The basis sets used here were of the augmented correlation-consistent polarized core-valence variety.   For the F, Li, and Na atoms, the all-electron aug-cc-pCVnZ (n = D, T, Q) basis sets were chosen,[37,38,39] while for the H atom the aug-cc-pVnZ sets were chosen[40] since H has no core orbitals.   The aug-cc-pVQZ basis sets for H may be designated (7s4p3d2f)/[5s4p3d2f], with the total number of contracted basis functions being 46, and the aug-cc-pCVQZ basis sets for F, Li and Na may be

3

designated (16s10p6d4f2g)/[9s8p6d4f2g], (16s10p6d4f2g)/[9s8p6d4f2g], and

(23s16p7d5f3g)/[10s9p7d5f3g], respectively, with the total numbers of contracted

basis functions being 109, 109 and 134, respectively. For the K, Rb and Cs atoms,

the inner core electrons were replaced by the Stuttgart-Cologne multiconfiguration

Dirac-Hartree-Fock (MCDHF) adjusted effective core potentials (ECP).[41] With

these ECPs, 10 core electrons $(1s^22s^22p^6)$ for K, 28 core electrons

$(1s^22s^22p^63s^23p^63d^{10})$ for Rb, and 46 core electrons $(1s^22s^22p^63s^23p^63d^{10}4s^24p^64d^{10})$

for Cs were included in the pseudopotentials. Building on these Stuttgart-Cologne

MCDHF ECPs, the augmented correlation-consistent polarized core-valence basis sets

aug-cc-pCVnZ-PP (n = D, T, Q), newly developed by Peterson and coworker,[42] were

employed in this study. The aug-cc-pCVQZ-PP basis sets for K and Rb have the

same numbers of primitive gaussian functions and contraction scheme, i.e.,

(18s15p11d5f3g)/[10s9p8d5f3g], and the aug-cc-pCVQZ-PP basis set for Cs could be

designated (18s15p11d8f3g)/[10s9p8d6f3g]. The numbers of contracted functions

for these pseudopotential incorporating basis sets are 139, 139, and 146 for K, Rb and

Cs, respectively. The total numbers of the aug-cc-pCVQZ(-PP) contracted gaussian

functions were 310 ($H_2\cdots$FLi), 335 ($H_2\cdots$FNa), 340 ($H_2\cdots$FK), 340 ($H_2\cdots$FRb), and 347

($H_2\cdots$FCs).

All the CCSD(T) and CCSDT computations were carried out with the CFOUR

program package.[43,44] In the coupled cluster treatments, restricted Hartree-Fock

(RHF) orbitals were used, and no core orbitals were frozen since the core orbitals and

the valence orbitals are not clearly separated in some cases of this study.

3. Results and Discussion

3.1 The Geometries

3.1.1 The Linear Structures

Zhang et al. reported that all the atoms of the H-H···Y-M (Y = F, Cl, Br; M = Li, Na, K) geometries are in-line.[31] Thus, linear H-H···F-M (M = Li, Na, K, Rb, Cs) structures (Figure 1) were investigated firstly. Table 1 reports our optimized geometries for the linear H-H···F-M (M = Li, Na, K, Rb, Cs) structures by CCSD(T) method with various aug-cc-pCVnZ(-PP) (n = D, T, Q) basis sets. Since the formation of hydrogen bonds is usually associated with changes in the bond distances for the proton-donor and proton-acceptor, the isolated MF (M = Li, Na, K, Rb, Cs) diatomic molecules were also studied at the same level of theory, and are reported in Table 1 for comparison. The optimized bond length (0.742 Å) for the free H_2 molecule are also shown in Footnote a to Table 1, but using the CCSD method, as H_2 has only two electrons.

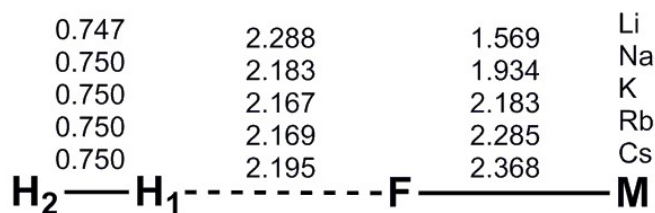| 0.747 | 2.288 | 1.569 | Li |
0.750	2.183	1.934	Na
0.750	2.167	2.183	K
0.750	2.169	2.285	Rb
0.750	2.195	2.368	Cs

$H_2 — H_1 - - - - - - - F —————— M$

Figure 1. Optimized linear H-H···F-M (M = Li, Na, K, Rb, Cs) structures with the CCSD(T)/aug-cc-pCVQZ(-PP) method. In Figure 1 and 2, all the distances are reported in Å.

As shown in Table 1, good convergence is seen with respect to the size of the basis sets. The equilibrium CCSD(T)/aug-cc-pCVQZ(-PP) bond distances (r_e) for

isolated MF (M = Li, Na, K, Rb, Cs) molecules are 1.567, 1.931, 2.177, 2.278, and

2.358 Å, respectively, in good agreement with the experimental r_e results of 1.564,

1.926, 2.172, 2.270, and 2.345 Å,[45] respectively, the differences being only 0.003,

0.005, 0.005, 0.008, and 0.013 Å. Our predicted H-H distance for the free H_2 is

0.742 Å, in very good agreement with the experimental r_e of 0.7414 Å.[46]

Table 1. Optimized bond distances (R_{H-H}, $R_{F...H}$ and R_{M-F}, in Å) and imaginary harmonic vibrational frequencies (ν_{Imag}) for the linear H-H···F-M (M = Li, Na, K, Rb, Cs) structures using the CCSD(T) method with various aug-cc-pCVnZ(-PP) (n = D, T, Q) basis sets.   Optimized bond distances (Diatomic M-F, in Å) for isolated MF diatomic molecules are also shown for comparison.   The dissociation energies (D_e, in kcal mol^{-1}) are based on the formula $D_e = E_{H2} + E_{MF} - E_{complex}$,[a] with the CCSD(T) and CCSDT methods.

Complex	Basis set	R_{M-F}	$R_{F...H}$	R_{H-H}	Diatomic M-F	ν_{Imag}	CCSD(T) D_e	CCSDT D_e
H-H···F-Li	aug-cc-pCVDZ	1.597	2.305	0.766	1.596	30i,30i	1.78	1.79
	aug-cc-pCVTZ	1.577	2.287	0.748	1.574	none	1.67	1.67
	aug-cc-pCVQZ	1.569	2.288	0.747	1.567	none	1.60	1.61
	Exp.				1.564[b]			
H-H···F-Na	aug-cc-pCVDZ	1.955	2.218	0.769	1.950	none	2.42	2.44
	aug-cc-pCVTZ	1.941	2.181	0.750	1.939	13i,13i	2.31	2.32
	aug-cc-pCVQZ	1.934	2.183	0.750	1.931	none	2.18	2.20
	Exp.				1.926[b]			
H-H···F-K	aug-cc-pCVDZ(-PP)	2.231	2.178	0.770	2.226	23i,23i	2.69	2.70
	aug-cc-pCVTZ(-PP)	2.197	2.163	0.751	2.191	none	2.44	2.46
	aug-cc-pCVQZ(-PP)	2.183	2.167	0.750	2.177	none	2.32	2.34
	Exp.				2.172[b]			
H-H···F-Rb	aug-cc-pCVDZ(-PP)	2.336	2.167	0.770	2.328	8i,8i	2.83	2.84
	aug-cc-pCVTZ(-PP)	2.298	2.162	0.751	2.292	none	2.47	2.49
	aug-cc-pCVQZ(-PP)	2.285	2.169	0.750	2.278	4i,4i	2.31	2.33
	Exp.				2.270[b]			
H-H···F-Cs	aug-cc-pCVDZ(-PP)	2.446	2.148	0.770	2.439	16i,16i	3.01	3.03
	aug-cc-pCVTZ(-PP)	2.384	2.193	0.751	2.375	none	2.33	2.35
	aug-cc-pCVQZ(-PP)	2.368	2.195	0.750	2.358	none	2.16	2.18
	Exp.				2.345[b]			

[a] Optimized bond distances for the free H_2 molecule are 0.762, 0.743 and 0.742 Å at the CCSD/aug-cc-pVDZ, CCSD/ aug-cc-pVTZ and CCSD/aug-cc-pVQZ levels, respectively.

[b] From Ref. [45]

The CCSD(T)/aug-cc-pCVQZ(-PP) F-M bond distances in the linear H-H···F-M (M = Li, Na, K, Rb, Cs) structures are 1.569, 1.934, 2.183, 2.285, and 2.368 Å, respectively. Compared to the isolated diatomic molecules, these distances are longer by 0.002 (Li-F), 0.003 (Na-F), 0.006 (K-F), 0.007 (Rb-F), and 0.010 Å (Cs-F), respectively. In this sense, the complex formation slightly weakens the M-F bonds. The corresponding H-H distances in these systems are 0.747, 0.750, 0.750, 0.750, and 0.750, also slightly longer than that in free H_2 molecule, namely 0.742 Å. The noncovalent interaction in linear H-H···F-M slightly weakens the H-H bond, with the H-H bond distances increasing by 0.07 Å (M = Li) or 0.08 Å (M = Na, K, Rb, Cs).

The hydrogen bond distances (H···F) in the linear H-H···F-M structures are 2.288, 2.183, 2.167, 2.169, and 2.195 Å for M = Li, Na, K, Rb, Cs, respectively, at the CCSD(T)/aug-cc-pCVQZ(-PP) level, longer than the conventional H···F hydrogen bonding distance (1.829 Å for the HF dimer),[47] suggesting a weak HB in the H-H···F-M system. On the other hand, the H···F distances in linear H-H···F-M decrease when the alkali metal M goes down from Li to K, but very slightly increase for Rb, and substantially increase for Cs. The strength of the hydrogen bonds in the H-H···F-M systems is related to the dipole moment of the isolated M-F molecule, and this will be discussed below in Section 3.4.

3.1.2 The Bent Structures

Although linear H-H···F-M (M = Li, Na, K, Rb, Cs) structures have almost all real vibrational frequencies (Table 1), indicating they are minima on their potential energy surfaces, our further CCSD(T) investigations find bent H-H···F-M (M = Li, Na, K, Rb, Cs) structures (Figure 2) having even lower energies. Compared to the

corresponding linear structures, the bent H-H⋯F-M (M = Li, Na, K, Rb, Cs) structures are lower in energy by 1.14, 0.76, 0.65, 0.56 and 0.31 kcal mol^{-1}, respectively, at the CCSD(T)/aug-cc-pCVQZ(-PP) level of theory.   Table 2 reports our optimized bent structures for the H-H⋯F-M (M = Li, Na, K, Rb, Cs) systems by CCSD(T) method with various aug-cc-pCVnZ(-PP) (n = D, T, Q) basis sets.   Again, good convergence is seen with respect to the size of the basis sets.

Table 2. Optimized geometries (bond distance R_{H1-H2}, $R_{F\cdots H1}$ and R_{M-F} in Å; bond angle $A_{M-F\cdots H1}$ and $A_{F\cdots H1-H2}$ in degree) and imaginary harmonic vibrational frequencies (ν_{Imag}) for the bent H-H⋯F-M (M = Li, Na, K, Rb, Cs) structures using CCSD(T) method with various aug-cc-pCVnZ(-PP) (n = D, T, Q) basis sets.   Optimized bond distances (R_{M-F}, in Å) for isolated MF diatomic molecules are also shown for comparison.   The dissociation energies (D_e, in kcal mol^{-1}) were derived from the formula $D_e = E_{H2} + E_{MF} - E_{complex}$.[a]

Complex	Basis set	R_{M-F}	$R_{F\cdots H}$	R_{H-H}	$A_{M-F\cdots H1}$	$A_{F\cdots H1-H2}$	Diatomic M-F	ν_{Imag}	CCSD(T) D_e	CCSDT D_e
H-H⋯F-Li	aug-cc-pCVDZ	1.600	2.671	0.765	50.2	126.6	1.596	None	3.15	3.16
	aug-cc-pCVTZ	1.581	2.546	0.750	52.2	130.9	1.574	None	2.83	2.85
	aug-cc-pCVQZ	1.574	2.566	0.749	51.7	129.6	1.567	None	2.74	2.76
	Exp.						1.564[b]			
H-H⋯F-Na	aug-cc-pCVDZ	1.962	2.152	0.773	71.1	157.5	1.950	None	2.99	3.01
	aug-cc-pCVTZ	1.952	2.155	0.755	69.6	155.2	1.939	None	3.09	3.12
	aug-cc-pCVQZ	1.943	2.158	0.754	69.3	154.2	1.931	None	2.94	2.96
	Exp.						1.926[b]			
H-H⋯F-K	aug-cc-pCVDZ(-PP)	2.242	2.100	0.775	76.9	161.7	2.226	None	3.51	3.53
	aug-cc-pCVTZ(-PP)	2.207	2.110	0.756	76.7	161.4	2.191	None	3.15	3.18
	aug-cc-pCVQZ(-PP)	2.193	2.119	0.754	76.7	160.0	2.177	None	2.97	3.00
	Exp.						2.172[b]			
H-H⋯F-Rb	aug-cc-pCVDZ(-PP)	2.347	2.088	0.775	80.1	166.5	2.328	None	3.38	3.41
	aug-cc-pCVTZ(-PP)	2.309	2.119	0.755	80.0	163.4	2.292	None	3.03	3.05
	aug-cc-pCVQZ(-PP)	2.295	2.133	0.754	79.8	161.5	2.278	None	2.87	2.89
	Exp.						2.270[b]			
H-H⋯F-Cs	aug-cc-pCVDZ(-PP)	2.459	2.114	0.773	83.3	170.4	2.439	None	3.28	3.30
	aug-cc-pCVTZ(-PP)	2.394	2.182	0.753	84.8	164.5	2.375	None	2.64	2.66
	aug-cc-pCVQZ(-PP)	2.377	2.199	0.751	85.1	162.8	2.358	None	2.47	2.49
	Exp.						2.345[b]			

[a] Optimized bond distances and total energies for H_2 molecules are 0.762, 0.743, 0.742 Å at the CCSD/aug-cc-pVDZ, CCSD/aug-cc-pVTZ and CCSD/aug-cc-pVQZ levels, respectively.
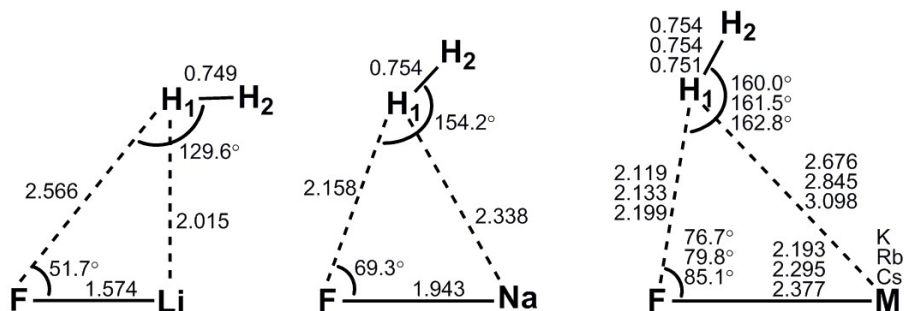
[b] From Ref. [45]

Figure 2. Optimized bent H-H⋯F-M (M = Li, Na, K, Rb, Cs) structures with the CCSD(T)/aug-cc-pCVQZ(-PP) method.   The relative energies of the bent H-H⋯F-M (M = Li, Na, K, Rb, Cs) structures are -1.14, -0.76, -0.65, -0.56, -0.31 kcal mol^{-1}, respectively, compared with the corresponding linear H-H⋯F-M structures.

The CCSD(T)/aug-cc-pCVQZ(-PP) F-M bond distances in the bent H-H⋯F-M (M = Li, Na, K, Rb, Cs) structures are 1.574, 1.943, 2.193, 2.295, and 2.377 Å, respectively.   Compared to the corresponding linear H-H⋯F-M structures, these distances are longer by 0.005 (F-Li), 0.009 (F-Na), 0.010 (F-K), 0.010 (F-Rb), and 0.009 Å (F-Cs), respectively.   Thus, the bent complex formation weakens the MF bonds even more.   The corresponding H-H distances in the bent H-H⋯F-M structures are 0.749, 0.754, 0.754, 0.754, and 0.751, respectively, also slightly longer than those in the linear H-H⋯F-M structures.   Thus, the noncovalent interaction in the bent H-H⋯F-M structures also weaken the H-H bond, with the H-H bond distances increasing by ~0.01 Å.

The H⋯F hydrogen bond distances in the bent H-H⋯F-M (M = Li, Na, K, Rb, Cs) structures are 2.566, 2.158, 2.119, 2.133, and 2.199 Å, respectively, at the CCSD(T)/aug-cc-pCVQZ(-PP) level.   Compared to the corresponding H⋯F distances in the linear H-H⋯F-M structures, these distances change by +0.278, -0.025, -0.048, -0.036, and +0.004 Å, respectively.   Especially, the bent H-H⋯F-Li structure

9

can also be regarded as a H-H···Li-F structure, since its H···Li distance is only 2.015 Å

(Figure 2).   The H···F hydrogen bond distances in the bent H-H···F-M structures are

also longer than the conventional H···F hydrogen bonding distance (1.829 Å for the

HF dimer)[47], suggesting weak HBs in the bent H-H···F-M system.   Similar to the

linear H-H···F-M structures, the bent H-H···F-M structures also have their H···F

distances decrease when the alkali metal M goes down from Li to K, but very slightly

increase for Rb, and substantially increase for Cs.

3.2 The Energies

Table 1 and 2 also presents dissociation energies (D_e) between a H_2 molecule and

a series of alkali halides.   The dissociation energies are derived from the following

formula:

$$D_e = E_{H2} + E_{MF} - E_{complex}$$

The total energies for the linear/bent H-H···F-M structures, as well as the isolated H_2

and MF diatomic molecules, are shown in Table S1/S2 (Supporting Information).

The dissociation energies for the linear H-H···F-M (M = Li, Na, K, Rb, Cs) structures

(Table 1) are 1.60, 2.18, 2.32, 2.31, and 2.16 kcal mol^{-1}, respectively, at the

CCSD(T)/aug-cc-pCVQZ(-PP) level of theory, with the CCSDT/aug-cc-pCVQZ(-PP)

single point computations give almost same results, i.e., 1.61, 2.20, 2.34, 2.33, and

2.18 kcal mol^{-1}, respectively.   The dissociation energies for the bent H-H···F-M (M =

Li, Na, K, Rb, Cs) structures (Table 2) are 2.74, 2.94, 2.97, 2.87, and 2.47 kcal mol^{-1},

respectively, at the CCSD(T)/aug-cc-pCVQZ(-PP) level, and 2.76, 2.96, 3.00, 2.89,

and   2.49   kcal   mol^{-1},   respectively,   at   the   CCSDT/aug-cc-pCVQZ(-PP)//

CCSD(T)/aug-cc-pCVQZ(-PP) level.   These dissociation energies fall in the order

Li < Na < K > Rb > Cs, which is consistent with the order of the HB distances

reported in Section 3.1.   Overall, these noncovalent dissociation energies are much

smaller than that for the water dimer (5.41 kcal mol^{-1} at the CCSD(T)/cc-pVQZ level).

Instead, these dissociation energies are more comparable with the C-H/π and N-H/π

interactions,[8] in the range of weak hydrogen bond interactions.[48]

3.3 The Vibrational Frequencies

Table 3 shows bond stretching vibrational frequencies for the linear H-H···F-M

(M = Li, Na, K, Rb, Cs) structures, the isolated H_2 and MF molecules using the

CCSD(T) method with the aug-cc-pCVQZ(-PP) basis set.   All vibrational harmonic

frequencies with their infrared intensities are shown in Table S3 (Supporting

Information).   The CCSD/aug-cc-pVQZ harmonic vibrational frequency for the free

H_2 is 4403 cm^{-1}, in excellent agreement with the experiment 4401.2 cm^{-1}.[46]   The

vibrational   frequencies   for   the   isolated   MF   molecules   at   the

CCSD(T)/aug-cc-pCVQZ(-PP) level are 531, 423, 370, and 349 cm^{-1} for M = Na, K,

Rb, Cs, respectively, in good agreement with the experimental harmonic frequencies

(536, 426, 373, and 353 cm^{-1}, respectively) with small error bars (less than ±0.35

cm^{-1}).[45]   For isolated LiF, our theoretical vibrational frequency 907 cm^{-1} is consistent

with the recently reported experimental value 910.6 cm^{-1} (Table 3).[49]

With the formation of the linear H-H···F-M (M = Li, Na, K, Rb, Cs) structures,

the H-H bond stretching vibrational frequencies for linear H-H···F-M decrease, in the

order 4324, 4270, 4258, 4258, 4272 cm^{-1}, respectively, for M = Li, Na, K, Cs, at

the CCSD(T)/aug-cc-pCVQZ(-PP) level of theory.   For the potassium and rubidium complexes, we see that the shifts in the H-H stretching are substantial, 145 (= 4403 – 4258) cm^{-1}.   The M-F stretching frequencies for the linear H-H$\cdots$F-M complexes are almost unchanged, being only -6, -1, -1, +2, +1 cm^{-1} compared with those for the isolated MF (M = Li, Na, K, Rb, Cs) diatomic molecules.

Table 3. The stretching vibrational frequencies (ν_{H-H}, $\nu_{F\cdots H}$ and, ν_{M-F} in cm^{-1}) for the H-H, H$\cdots$F, and F-M bonds in the linear H-H$\cdots$F-M (M = Li, Na, K, Rb, Cs) structures using the CCSD(T) method with the aug-cc-pCVQZ(-PP) basis function.   The stretching vibrational frequencies (Diatomic ν_{M-F}) for the isolated M-F diatomic molecules are also given for comparison.[a] $\Delta\nu_{H-H}$ and $\Delta\nu_{M-F}$ show the shifts of the H-H and F-M bond stretching frequencies, respectively.   The dipole moments for the complexes ($\mu_{complex}$, in Debye) and for the isolated MF (Diatomic μ_{MF}, in Debye) are reported also.

Complex	Basis set	ν_{H-H}	$\Delta\nu_{H-H}$	$\nu_{F\cdots H}$	ν_{M-F}	$\Delta\nu_{M-F}$	Diatomic ν_{M-F}	$\mu_{complex}$	Diatomic μ_{MF}
H-H$\cdots$F-Li	aug-cc-pCVQZ	4324	-79	214	901	-6	907	6.69	6.30
	Exp.						910.6[b]		6.33[d]
H-H$\cdots$F-Na	aug-cc-pCVQZ	4270	-133	242	530	-1	531	8.67	8.17
	Exp.						536.10±0.35[c]		8.16[d]
H-H$\cdots$F-K	aug-cc-pCVQZ(-PP)	4258	-145	245	422	-1	423	9.20	8.63
	Exp.						426.04±0.24[c]		8.59[d]
H-H$\cdots$F-Rb	aug-cc-pCVQZ(-PP)	4258	-145	241	372	+2	370	9.17	8.58
	Exp.						373.27±0.08[c]		8.55[d]
H-H$\cdots$F-Cs	aug-cc-pCVQZ(-PP)	4272	-131	233	350	+1	349	8.55	7.94
	Exp.						352.56±0.04[c]		7.88[d]

[a] The H-H bond stretching vibrational frequency for H$_2$ diatomic molecule is 4403 cm^{-1} at the CCSD/aug-cc-pVQZ level.   The experimental stretching vibrational frequencies for H$_2$ molecule is 4401.2 cm^{-1} (Ref. [46]).
[b] From Ref. [49].
[c] From Ref. [45].
[d] From Ref. [50].

The vibrational frequency for the H$\cdots$F stretching mode in the linear H-H$\cdots$F-M structures becomes greater as the alkali metal M goes down from Li (214 cm^{-1}) to Na (242 cm^{-1}) to K (245 cm^{-1}), but slightly lower for M = Rb (241 cm^{-1}) and significantly

lower for M = Cs (233 cm^{-1}).   Again, the vibrational frequencies for the hydrogen

bond stretching mode suggest that the HB is stronger in the H-H···F-M system from

M = Li to K, but slightly weaker for M = Rb, and much weaker for M = Cs, consistent

with the results of the bond distances and bond energies, discussed above.

Table 4 shows bond stretching vibrational frequencies for the bent H-H···F-M (M

= Li, Na, K, Rb, Cs) structures using the CCSD(T) method with the

aug-cc-pCVQZ(-PP) basis set.   With the formation of the bent H-H···F-M structures,

the H-H bond stretching vibrational frequencies become even lower, in the order 4305,

4193, 4186, 4198, 4241 cm^{-1}, respectively, for M = Li, Na, K, Rb, Cs, at the

CCSD(T)/aug-cc-pCVQZ(-PP) level of theory.   The potassium complex has the

largest H-H bond stretching frequency shift of 217 (= 4403 − 4186) cm^{-1}.   The M-F

stretching frequencies for the bent H-H···F-M structures are also somewhat lower,

being -9, -12, -7, -7, -7 cm^{-1} compared with those for corresponding linear H-H···F-M

structures, or -15, -13, -8, -5, -6 cm^{-1} compared with those the isolated MF (M = Li,

Na, K, Rb, Cs) diatomic molecules.

The vibrational frequency for the H···F stretching mode in the bent H-H···F-M

structures becomes lower as the alkali metal M goes down from Li (344 cm^{-1}) to Na

(267 cm^{-1}) to K (263 cm^{-1}) to Rb (257 cm^{-1}) and to Cs (241 cm^{-1}).   It should be noted

that the bent H-H···F-Li structure, and to some extent the bent H-H···F-Na structure,

are much different from other bent H-H···F-M structures.   For the similar bent

structure of the H-H···F-M (M = K, Rb, Cs) systems, the vibrational frequencies for

the H···F hydrogen bond stretching mode suggest that the HB becomes weaker for the

H-H···F-M systems from M = K to Cs, consistent with the results of the bond distances and bond energies, discussed above.

Table 4. The stretching vibrational frequencies (ν_{H-H}, $\nu_{F...H}$ and, ν_{M-F} in cm^{-1}) for the H-H, H···F, and F-M bonds in the bent H-H···F-M (M = Li, Na, K, Rb, Cs) structures using the CCSD(T) method with the aug-cc-pCVQZ(-PP) basis function. $\Delta\nu_{H-H}$ and $\Delta\nu_{M-F}$ show the shifts of the H-H and F-M bond stretching frequencies, respectively.[a] The dipole moments for the complexes ($\mu_{complex}$, in Debye) are reported also.[b]

Complex	Basis set	ν_{H-H}	$\Delta\nu_{H-H}$	$\nu_{F...H}$	ν_{M-F}	$\Delta\nu_{M-F}$	$\mu_{complex}$ (X)	$\mu_{complex}$ (Y)
H2-H1···F-Li	aug-cc-pCVQZ	4305	*-98*	344	892	*-15*	5.69	2.33
H2-H1···F-Na	aug-cc-pCVQZ	4193	*-210*	267	518	*-13*	7.81	0.19
H2-H1···F-K	aug-cc-pCVQZ(-PP)	4186	*-217*	263	415	*-8*	8.39	0.21
H2-H1···F-Rb	aug-cc-pCVQZ(-PP)	4198	*-205*	257	365	*-5*	8.41	0.33
H2-H1···F-Cs	aug-cc-pCVQZ(-PP)	4241	*-162*	241	343	*-6*	7.89	0.44

[a] See Table 3 for the stretching vibrational frequencies of isolated MF and H_2 diatomic molecules.
[b] See Table 3 for the dipole moments of isolated MF diatomic molecules.

3.4 The Dipole Moments

Tables 3 and 4 also show the dipole moments for the linear/bent H-H···F-M (M = Li, Na, K, Rb, Cs) structures and the isolated MF molecules. The strength of traditional HB is thought to be related to the dipole-dipole interaction between proton donor and proton acceptor. Large dipole moments would thus lead to strong HB. Though the free H_2 molecule has zero dipole moment, when approaching the strongly polarized alkali halide complexes MF, an induced dipole occurs. As shown in Tables 3 and 4, the CCSD(T)/aug-cc-pCVQZ(-PP) dipole moments for the isolated diatomic MF (M = Li, Na, K, Rb, Cs) molecules are 6.30, 8.17, 8.63, 8.58, and 7.94 Debye, respectively, which agree well with corresponding experimental values of 6.33, 8.16, 8.59, 8.55, and 7.88 Debye.[50] The MF dipole moments increase as the alkali metal goes from Li to K, but slightly decrease for M = Rb, and further decrease

for M = Cs.   This is consistent with the order of the HB strength, the bond distances, the bond energies, and the vibrational frequencies discussed above.   The theoretical dipole moments for the linear H-H···F-M (M = Li, Na, K, Rb, Cs) structures are 6.69, 8.67, 9.20, 9.17, and 8.55 Debye (Table 3), respectively, somewhat larger (by 0.4 – 0.6 Debye) than those for the isolated MF.   The theoretical dipole moments for the bent H-H···F-M (M = Li, Na, K, Rb, Cs) structures are (μ_x = 5.69, μ_y = 2.33), (7.81, 0.19), (5.69, 2.33), (5.69, 2.33), and (5.69, 2.33) Debye (Table 4), respectively, somewhat smaller than those for the isolated MF.   Note, however, that all of our results are contrary to the general chemistry idea the CsF is the most polar known diatomic molecule.

3.5 The Atomic Charges

Table 5 shows the natural charges for the isolated MF molecules and the bent H-H···F-M (M = Li, Na, K, Rb, Cs) structures using natural bond orbital (NBO)[51,52,53,54] analysis based on Hartree-Fock orbitals.   Although the atomic charges for the hydrogen atoms in the free H_2 molecule are necessarily zero, for the complex the charge of the H atom adjacent to F atom in H-H···F-M is positive with values 0.05, 0.08, 0.08, 0.08, and 0.07, induced by the polarity of the alkali halide, while the other H atom is negative.   The total charge of the H_2 moiety in the H-H···F-M molecule becomes slightly negative.   Thus, with the hydrogen bond formation in the natural charge picture, very small negative charge (< 0.02) transfers from the MF moiety (proton acceptor) to the H_2 moiety (proton donor).

Table 5. Natural charges (q_{H2}, q_{H1}, q_F and q_M) for the bent H-H···F-M (M = Li, Na, K, Rb, Cs) structures using NBO analysis based on Hartree-Fock orbitals. The natural atomic charges (Diatomic q_F and q_M) for isolated MF diatomic molecules are also shown for comparison.

Complex	Basis set	q_{H2}	q_{H1}	q_F	q_M	Diatomic q_F	Diatomic q_M
H2-H1···F-Li	aug-cc-pCVQZ	-0.05	0.05	-0.97	0.97	-0.98	0.98
H2-H1···F-Na	aug-cc-pCVQZ	-0.09	0.08	-0.98	0.99	-0.99	0.99
H2-H1···F-K	aug-cc-pCVQZ(-PP)	-0.10	0.08	-0.97	0.98	-0.98	0.98
H2-H1···F-Rb	aug-cc-pCVQZ(-PP)	-0.10	0.08	-0.97	0.98	-0.98	0.98
H2-H1···F-Cs	aug-cc-pCVDZ(-PP)	-0.09	0.07	-0.97	0.98	-0.98	0.98

3.6 The symmetry-adapted perturbation theory energy decompositions

Symmetry-adapted perturbation theory (SAPT) [55] was used to explore the intermolecular interactions binding the MF and H_2 monomers as a means of explaining the preference for a bent structure (Figure 2) over the linear structure (Figure 1) studied previously.[31] The MF-H_2 interaction energies (ΔE_{int}) were decomposed into the electrostatic (ΔE_{elst}), induction (ΔE_{ind}), dispersion (ΔE_{disp}), exchange (ΔE_{exch}) components using SAPT implemented in MOLPRO 2010.1.[56] This research employed the lowest-order SAPT truncation (SAPT0) consisting of the following energy expressions:

$$\Delta E_{elst} = \Delta E_{elst}^{(10)},$$

$$\Delta E_{ind} = \Delta E_{ind,resp}^{(20)} + \Delta E_{exch-ind,resp}^{(20)} + \delta_{HF}^{(2)},$$

$$\Delta E_{disp} = \Delta E_{disp}^{(20)} + \Delta E_{exch-ind,resp}^{(20)}, \text{ and}$$

$$\Delta E_{exch} = \Delta E_{exch}^{(10)},$$

where

$$\delta_{HF}^{(2)} = \Delta E_{int}^{HF} - \left(\Delta E_{elst}^{(10)} + \Delta E_{exch}^{(10)} + \Delta E_{ind,resp}^{(20)} + \Delta E_{exch-ind,resp}^{(20)} \right)$$

provides an estimate of higher-order inductive effects needed for treating the ionic MF monomer. Above, v and w in $\Delta E^{(vw)}$ denote the expansion of the order of the

intermonomer interaction ($\hat{V}$) and intramonomer correlation ($\hat{W}$) operators, respectively. The *resp* subscript denotes that orbital relaxation is included. Note that the *w*-index in each term is equal to zero, which indicates that intramonomer correlation has been ignored; only contributions from intermonomer interactions have been considered. Hartree-Fock wave functions were used throughout. The cc-pVTZ basis set was employed for the H, F, Li, and Na atoms and the cc-pVTZ-PP basis sets and effective core potentials were employed for the K, Rb, and Cs atoms. This SAPT0 treatment yielded ΔE_{int} values that are qualitatively similar to the high-level coupled cluster energies.
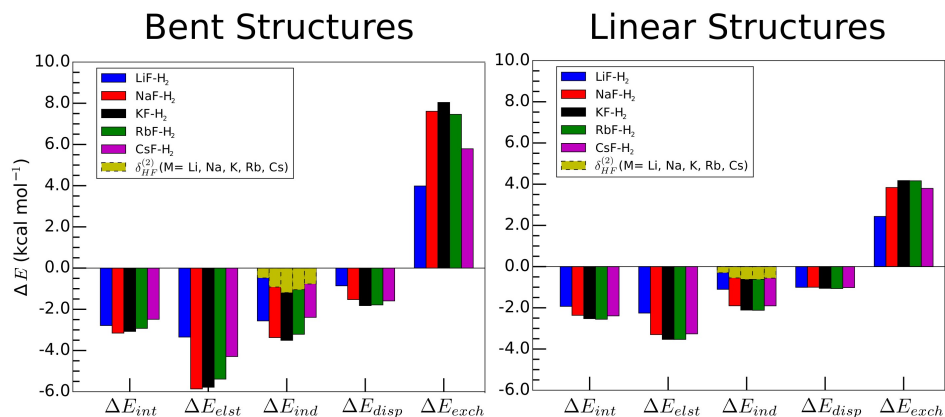
Figure 3. SAPT0 decomposition of the MF-H$_2$ (M = Li, Na, K, Rb, Cs) interaction energies (ΔE_{int}) for the bent structures (left) and linear structures (right). We emphasize the importance of higher-order contributions to the induction energies by plotting the values of the $\delta_{HF}^{(2)}$ terms as gold, dashed bars on top of the induction results.

The SAPT0/cc-pVTZ interaction energies for both the bent and linear H-H···F-M structures are plotted in Figure 3 and are explicitly tabulated in Table S5 and Table S6 (Supporting Information), respectively. Figure 3 shows a trend commonly seen from

SAPT: the attractive electrostatic, induction, and dispersion energies decrease concomitantly with increases to the exchange energy. As such, the H-H···F-M ΔE_{int} values wind up narrowly distributed over a 0.7 kcal mol^{-1} range.

The distribution of energies for the bent and linear structures are similar, in that the ΔE_{elst}, ΔE_{ind}, ΔE_{disp}, ΔE_{exch} terms do not trend monotonically with the size of the alkali metal. The bent structures exhibit a greater variance in the energies for a given SAPT0 component as M changes, whereas the distributions for the linear structures are flatter. The difference in energy distributions is undoubtedly related to the bent structures being optimized with the additional M-H1-H2 and F-M-H1 angles as degrees of freedom. More importantly, as we will now discuss, bending these two angles allows for additional favorable electrostatic and induction interactions to arise which are not present in the linear structures. Since electrostatic and induction together constitute ~85% of the total attractive interaction energy for all species, these additional interactions lower the interaction energies for the bent structures, making them more favorable.

The electrostatic energy results from the sum of two potentially cooperative interactions involving the σ(H$_2$) electron density and either the M$^+$ or F$^-$ ion. The existence of one or both interactions depends on the overall structure. To most simply understand the electrostatic interactions, we need only consider the electrostatic potential of H$_2$, which was computed by Grabowski, Alkorta, and Elguero.[57] The potential is described by an ellipsoid with a region of positive potential at each H nuclei (a σ-hole) and a region of negative potential centered between the two H nuclei where

the $\sigma(H_2)$ electron density is greatest.

Electrostatic attraction in the linear structures is largely limited to the interaction of the F^- ion and the positively-charged σ-hole of the $\sigma(H_2)$-centered potential. Meanwhile, the bent structures can experience an attractive $[\sigma(H_2)]^{\delta-}/M^+$ interaction, since the bulk of the $\sigma(H_2)$ electron density (perpendicular to the H_2 axis) is oriented directly towards the M^+ ion. In addition, Figure 2 shows that the bent structures still have the H_2 internuclear axis partially oriented towards the F^- ion, suggesting that the bent structures still make use of the attractive $(\sigma\text{-hole})^{\delta+}/F^-$ interaction. This interaction should be particularly prominent for M = Na, K, and Rb, where the increased M-H1-H2 angle even more greatly orients the σ-hole towards the F^- ion. Lastly, we note that the surprising strength of either these electrostatic interactions is in part due to the significant charge of the ions of the MF dipole ($\geq |0.96|$; see Table 5).

Similar to the electrostatic component, the induction energy of the bent structures becomes larger in absolute value relative to the induction energy of the linear structures because of additional attractive interactions. To understand this, we recognize that the induction term is dictated by two different types of interactions. The first type of interest -- that most readily explains the preference for the bent structures -- involves intermolecular donor-acceptor interactions. There are two cooperative donor-acceptor interactions that are important in the MF-H_2 species: (1) $n(F^-) \rightarrow \sigma^*(H_2)$ and (2) $\sigma(H_2) \rightarrow s^*(M^+)$. The presence of both of these interactions is readily confirmed by comparing the delocalization energies [*E(2)*] from the second-order perturbation theory analysis[53] that was computed with the *NBO 6.0* package.[54] The

E(2) values for these interactions are reported in Table S7 of the Supporting Information; below we discuss a qualitative picture provided by these values.

Nonzero *E(2)* values exist when the $n(F^-) \rightarrow \sigma^*(H_2)$ interaction is present in both the bent and linear structures. With the exception of LiF-H_2, we found this interaction to be appreciably stronger in the bent structures. This result is somewhat unintuitive: one may expect the interaction in the linear structures to be equally competitive, if not stronger than the interaction in the bent structures. In the linear structures, the F^- ion has a *p*-orbital oriented along the molecular axis directly towards the $\sigma^*(H_2)$ orbital to facilitate charge-transfer; however, on the directly opposite side of the H_2 monomer is the M^+ ion, which also accepts charge from this same *p*-orbital. This secondary charge-transfer within the MF monomer may quench the intermolecular charge-transfer to some extent in the linear structures. In the case of the bent structures, all three F^- ion *p*-orbitals may be used to optimize charge-transfer. In the case of the $\sigma(H_2) \rightarrow s^*(M^+)$ interaction, moderately strong instances of this interaction are found in each of the bent structures. In contrast, this interaction is essentially absent from the linear structures with M = Li, Na, K (i.e., *E(2)* < 0.10 kcal mol^{-1}); even for M= Rb, Cs, the interaction in the linear structures is half as strong as that for the bent structures. A bent structure is generally required to facilitate orbital overlap between the $\sigma(H_2)$ and $s^*(M^+)$ orbitals since the $\sigma(H_2)$ electron density is found radially along axes perpendicular to the H-H axis; for the linear structures, the diminished $\sigma(H_2)$ electron density away from both hydrogen nuclei, parallel to the H-H axis, limits the potential strength of this interaction.

What is noteworthy, is that both of these charge-transfer mechanisms would act to weaken the H-H bond and lead to concomitant red-shift of the H-H stretch frequency, with respect to the free molecule H_2. Tables 1-2 (for the bond lengths) and Tables 3-4 (for the vibrational frequencies) indeed show both of these phenomena to occur. Moreover, the bent structures show greater shifts for these properties than the linear structures, in alignment with the fact that there is greater charge-transfer in the former set of structures.

The second interaction type is the more intuitive MF/H_2 dipole/induced-dipole interaction, which is present to some degree in both structures. From a basic multipole-expansion perspective, the dipole/induced-dipole interaction would be favored in the linear structure over the bent structure. Indeed, evidence for this notion can be found by comparing the dipole moments for the linear and bent structures in Tables 3 and 4, respectively: the dipoles shift greatly for the linear structures than the bent structures. In general, however, the low polarizability of the H_2 monomer should limit the magnitude of the strength of dipole/induced-dipole interactions in this system. The favorability for this interaction may explain why the difference between the induction energies of the bent and linear structures is not greater, as suggested by the charge-transfer results. Indeed, this idea implies the significance of charge-transfer in causing the $MF-H_2$ complexes to adopt a bent structure. Regardless, these induction interactions account for the appreciable shifts in the natural atomic charges in the bent structures (see Table 5).

Lastly, we emphasize the importance of including the higher-order contributions

contained within the $\delta_{HF}^{(2)}$ terms (listed in the caption of Figure 3). These terms appear to make up anywhere from 15-30% of the computed induction energy across all species. Therefore, this term should not be ignored during SAPT analyses for systems like MF-H_2.

The most striking contrast between the dispersion energies for the bent and linear structures is the distribution of these energies as M changes from Li to Cs. For the linear structures, each dispersion interaction energy is almost exactly -1.0 kcal mol^{-1}, whereas for the bent structures, the magnitude of the dispersion energies increase in absolute value from M = Li to K, then decreases again (similar to the other components). This trend is not altogether surprising. In the linear structures, the dispersion interaction is always limited to the interaction of the densities of the F$^-$ ion and the H1 atom of H_2; since the intermolecular F-H1 distance varies by only 0.1 Angstrom across all linear species, it is reasonable that the dispersion energy only changes by 0.1 kcal mol^{-1}. In the case, of the bent structures, more of the electron density of the σ-orbital can be placed alongside the MF monomer's electron density: this increases the opportunity to create more instantaneous dipoles compared to the linear structures. In either situation, however, the dispersion component will remain somewhat limited because there is so little density on H_2 to generate dispersion interactions.

Lastly, the significance of the exchange interactions can be discussed by their relation to the attractive components. To increase the strength of the above-discussed electrostatic, induction, and dispersion interactions, the MF and H_2 monomers are necessarily brought into closer contact, thus increasing the exchange repulsion. This

feature explains why the exchange energies of the bent structures are 2-4 kcal mol^{-1} greater than the energies for their linear analogs. As a result, the total interaction energies of the bent structures are only 0.3-1.1 kcal mol^{-1} lower than the linear structures, despite the former structures having a greater number of more attractive interactions.

4. Conclusions

A new type of hydrogen bond formed between the hydrogen molecule and the alkali halides, H-H···F-M (M = Li, Na, K, Rb, Cs), has been extensively investigated using the CCSD(T) and CCSDT methods in conjunction with augmented correlation-consistent polarized core-valence basis sets though quadruple zeta. Different from the linear H-H···F-M structures reported by Zhang et al., our CCSD(T) investigations predict the lowest energy H-H···F-M structures are in bent. The dissociation energies for bent H-H···F-M (M = Li, Na, K, Rb, Cs) systems are 2.76, 2.96, 3.00, 2.89, and 2.49 kcal mol^{-1}, respectively, at the most reliable CCSDT/aug-cc-pVQZ(-PP)//CCSD(T)/aug-cc-pVQZ(-PP) level of theory. These energies fall in the order Li < Na < K > Rb > Cs, indicating that the HH···FM hydrogen bonds become stronger when the alkali metal M goes down from Li to K, but weaker for M = Rb and Cs. This same order is seen in the predicted H···F bond distances and H···F vibrational stretching frequencies. The dipole moments for the isolated MF [6.3 (LiF), 8.2 (NaF), 8.6 (KF), 8.6 (RbF), and 7.9 (CsF) Debye] may explain this irregular order of the HH···FM hydrogen bond strengths.

Comparison of the H-H⋯F-M SAPT0 interaction energies for the bent and linear structures reveals that the preference for the bent structures arises from three significant factors. First, the bent structures undergo electrostatic attraction between the M^+ (F^-) and the negative (positive) potential of the $\sigma(H_2)$ electron density, where the positive potential is a σ-hole situated at the hydrogen nuclei. In contrast, the linear structures can only experience significant attraction from the $F^-/(\sigma\text{-hole})^+$ interaction. Second, we identified two intermolecular cooperative donor-acceptor interactions: (1) $n(F^-) \rightarrow \sigma^*(H\text{-}H)$ and (2) $\sigma(H\text{-}H) \rightarrow s^*(M^+)$ using the second-order perturbation theory analysis using natural bonding orbital theory. Using the $E(2)$ values from this method, we note that the first of these two interactions is generally stronger in the bent structures than for the linear structures. The second of these interactions is very weak, to the point of being essentially absent, in each linear structure. The final factor is that the bent structure allows more intermolecular surface-area contact, which increases the magnitude of the dispersion energy. In contrast, the dispersion term is largely the same in each of the linear structures. In each case, bending the M-H1-H2 and F-M-H1 angles orients the electron density of the H_2 monomer in such a way that grants the bent structures access to a greater number of attractive interactions, which are largely absent in the linear structures. In addition, optimization of these angular degrees of freedom helps fine-tune the strength of the strength of these interactions. It is hoped that the present comprehensive study will encourage new experiments.

Acknowledgements

Supporting Information

Table S1: Total energies for linear H-H···F-M (M = Li, Na, K, Rb, Cs) structures at the CCSD(T)/ aug-cc-pCVnZ and CCSDT/aug-cc-pCVnZ//CCSD(T)/aug-cc-pCVnZ (n = D, T, Q) levels of theory.   Total energies for isolated MF diatomic molecules are also shown for comparison.

Table S2: Total energies for bent H-H···F-M (M = Li, Na, K, Rb, Cs) structures at the CCSD(T)/ aug-cc-pCVnZ and CCSDT/aug-cc-pCVnZ//CCSD(T)/aug-cc-pCVnZ (n = D, T, Q) levels of theory.   Total energies for isolated MF diatomic molecules are also shown for comparison.

Table S3: Harmonic vibrational frequencies and infrared intensities for linear H-H···F-M (M = Li, Na, K, Rb, Cs) structures and isolated M-F diatomic molecules using the CCSD(T) method with various aug-cc-pCVnZ (n = D, T, Q) basis sets.

Table S4: Harmonic vibrational frequencies and infrared intensities for bent H-H···F-M (M = Li, Na, K, Rb, Cs) structures using the CCSD(T) method with various aug-cc-pCVnZ (n = D, T, Q) basis sets.

Table S5. The total interaction energy (ΔE_{int}) and the energies of each component (ΔE_{elst}, ΔE_{ind}, ΔE_{disp}, ΔE_{exch}) for the bent H-H···F-M (M = Li, Na, K, Rb, Cs) structures.   Each energy was computed at the SAPT0/cc-pVTZ level of theory and is in kcal mol^{-1}.   The parenthetical values denote what percentage of ΔE_{int} that the component comprises.

Table S6. The total interaction energy (ΔE_{int}) and the energies of each component (ΔE_{elst}, ΔE_{ind}, ΔE_{disp}, ΔE_{exch}) for the linear H-H···F-M (M = Li, Na, K, Rb, Cs) structures. Each energy was computed at the SAPT0/cc-pVTZ level of theory and is in kcal mol^{-1}.   The parenthetical values denote what percentage of ΔE_{int} that the component comprises.

Table S7. Donor-acceptor energies [$E(2)$] above 0.1 kcal mol^{-1} from the second-order perturbation theory analysis in NBO 6.0. Each instance of the given interaction are given below. For completeness, the $\sigma(H_2) \rightarrow s^*(M^+)$ interactions include those interactions for which the LV(Cs) *and* RY(Cs) orbital is an acceptor, since the latter was found to be similarly as strong as the former.

Table S8. Total energies ($E_{complex}$) and relative energies ($\Delta E_{complex}$) for the H-H···F-M (M = Li, Na, K, Rb, Cs) systems with various H-H···F angles obtained from relaxed potential energy surface scans at the CCSD(T)/aug-cc-pCVQZ(-PP) level of theory.

References

[1] Grabowski, S. J. What is the covalency of hydrogen bonding? *Chem. Rev.* **2011**, *111*, 2597-2625.

[2] Weinhold, F.; Klein, R. A. What is a hydrogen bond? Mutually consistent theoretical and experimental criteria for characterizing h-bonding interactions. *Mol. Phys.* **2012**, *110*, 565-579.

[3] Liu, Y. Z.; Hu, C. H.; Comotti, A.; Ward, M. D. Supramolecular archimedean cages assembled with 72 hydrogen bonds. *Science* **2011**, *333*, 436-440.

[4] Pauling, L. *The nature of the chemical bond*, Cornell University Press, 1939.

[5] Arunan, E.; Desiraju, G. R.; Klein, R. A.; Sadlej, J.; Scheiner, S.; Alkorta, I.; Clary, D. C.; Crabtree, R. H.; Dannenberg, J. J.; Hobza, P.; Kjaegaard, H. G.; Legon, A. C.; Mennucci, B.; Nesbitt, D. J. Definition of the hydrogen bond: an account (IUPAC technical report). *Pure Appl. Chem*. **2011**, *83*, 1619-1636.

[6] Holland, G. P.; Mou, Q.; Yarger, J. L. Determining hydrogen-bond interactions in spider silk with ^{1}H-^{13}C HETCOR fast MAS solid-state NMR and DFT proton chemical shift calculations. *Chem. Commun.* **2013**, *49*, 6680-6682.

[7] Sarkhel, S.; Desiraju, G. R. N-H⋯O, O-H⋯O, and C-H⋯O hydrogen bonds in protein-ligand complexes: strong and weak interactions in molecular recognition. *Proteins: Struct., Funct.,Bioinf.* **2004**, *54*, 247-259.

[8] Tsuzuki, S.; Honda, K.; Uchimaru, T.; Mikami, M.; Tanabe, K. Origin of the attraction and directionality of the NH/π interaction: comparison with OH/π and CH/π interactions. *J. Am. Chem. Soc.* **2000**, *122*, 11450-11458.

[9] Suzuki, S.; Green, P. G.; Bumgarner, R. E.; Dasgupta, S.; Goddard, W. A.; Blake, G. A. Benzene forms hydrogen bonds with water. *Science* **1992**, *257*, 942-945.

[10] Epstein, L. M.; Shubina, E. S. New types of hydrogen bonding in organometallic chemistry. *Coordin. Chem. Rev.* **2002**, *231*, 165-181.

[11] Mata, I.; Alkorta, I.; Molins, E.; Espinosa, E. Universal features of the electron density distribution in hydrogen-bonding regions: a comprehensive study involving H⋯X (X = H, C, N, O, F, S, Cl, π) interactions. *Chem. Eur. J.* **2010**, *16*, 2442-2452.

[12] Nishio, M. CH/π hydrogen bonds in crystals. *CrystEngComm* **2004**, *6*, 130-158.

[13] Dupont, J.; Suarez, P. A. Z.; De Souza, R. F.; Burrow, R. A.; Kintzinger, J. P. C-H-π interactions in 1-n-butyl-3-methylimidazolium tetraphenylborate molten salt: solid and solution structures. *Chem. Eur. J.* **2000**, *6*, 2377-2381.

[14] Tsuzuki, S.; Honda, K.; Uchimaru, T.; Mikami, M.; Tanabe, K. The magnitude of the CH/π interaction between benzene and some model hydrocarbons. *J. Am. Chem. Soc.* **2000**, *122*, 3746-3753.

[15] Brandl, M.; Weiss, M. S.; Jabs, A.; Sühnel, J.; Hilgenfeld, R. C-H⋯π interactions in proteins. *J. Mol. Biol.* **2001**, *307*, 357-377.

[16] Arduengo, A. J.; Gamper, S. F.; Tamm, M.; Calabrese, J. C.; Davidson, F.; Craig, H. A. A bis(carbene)-proton complex: structure of a C-H-C hydrogen bond. *J. Am. Chem. Soc.* **1995**, *117*, 572-573.

[17] Crabtree, R. H. A new type of hydrogen bond. *Science* **1998**, *282*, 2000-2001.

[18] Custelcean, R.; Jackson, J. E. Dihydrogen bonding: structures, energetics, and dynamics. *Chem. Rev.* **2001**, *101*, 1963-1980.

[19] Danovich, D.; Shaik, S.; Neese, F.; Echeverria, J.; Aullon, G.; Alvarez, S. Understanding the nature of the CH⋯HC interactions in alkanes. *J. Chem. Theory Comput.* **2013**, *9*, 1977-1991.

[20] He, M. X.; Zhang, R. Q.; Niehaus, T. A.; Frauenheim, Th.; Lee, S. T. Sensitivity of hydrogenated silicon nanodot on small polar molecules. *J. Theor. Comput. Chem.* **2009**, *8*, 299-316.

[21] Wolstenholme, D. J.; Flogeras, J.; Che, F. N.; Decken, A.; McGrady, G. S. Homopolar dihydrogen bonding in alkali metal amidoboranes: crystal engineering of low-dimensional molecular materials. *J. Am. Chem. Soc.* **2013**, *135*, 2439-2442.

[22] Wolstenholme, D. J.; Titah, J. T.; Che, F. N.; Traboulsee, K. T.; Flogeras, J.; McGrady, G. S. Homopolar dihydrogen bonding in alkali-metal amidoboranes and its implications for hydrogen storage. *J. Am. Chem. Soc.* **2011**, *133*, 16598-16604.

[23] Weinhold, F.; Klein, R. A. Anti-electrostatic hydrogen bonds. *Angew. Chem. Int. Ed.* **2014**, *53*, 11214-11217; *Angew. Chem.* **2014**, *126*, 11396-11399.

[24] Knorr, A.; Stange, P.; Fumino, K.; Weinhold, F.; Ludwig, R. Spectroscopic evidence for clusters of like-charged ions in ionic liquids stabilized by cooperative hydrogen bonding. *ChemPhysChem* **2016**, *17*, 458-462.

[25] Fatila, E. M.; Twum, E. B.; Sengupta, A.; Pink, M.; Karty, J. A.; Raghavachari, K.; Flood, A. H. Anions stabilize each other inside macrocyclic hosts. *Angew. Chem. Int. Ed.* **2016**, *55*, 14057-14062; *Angew. Chem.* **2016**, *128*, 14263-14268.

[26] Weinhold, F. Polyion covalency: exotic species from the unexplored world of electrostatically shielded molecular ion chemistry. *Angew. Chem. Int. Ed.* **2017**, *56*, 14577-14581; *Angew. Chem.* **2017**, *129*, 14769-14773.

[27] Wild, D. A.; Bieske, E. J. Infrared spectrum of the I^--D_2 anion complex. *J. Chem. Phys.* **2004**, *121*, 12276-12281.

[28] Wild, D. A.; Wilson, R. L.; Weiser, P. S.; Bieske, E. J. Rotationally resolved infrared spectrum of the Cl^--H_2 anion complex. *J. Chem. Phys.*, **2000**, *113*, 10154-10157.

[29] Wild, D. A.; Weiser, P. S.; Bieske, E. J.; Zehnacker, A. The $^{35}Cl^-$-H_2 and $^{35}Cl^-$-D_2 anion complexes: infrared spectra and radial intermolecular potentials. *J. Chem. Phys.*, **2001**, *115*, 824-832.

[30] Brammer, L. Metals and hydrogen bonds. *Dalton Trans.* **2003**, 3145-3157.

[31] Zhu, H. Y.; Huang, B. L.; Li, J. F.; Jiang, Z. Y.; Wang, B.; Wang, Z. G.; Zhang, R.-Q. Tunable dipole induced hydrogen bonds between a hydrogen molecule and alkali halides. *Phys. Chem. Chem. Phys.* **2015**, *17*, 20361-20367.

[32] Purvis, G. D.; Bartlett, R. J. A full coupled-cluster singles and doubles model: the inclusion of disconnected triples. *J. Chem. Phys.* **1982**, *76*, 1910-1918.

[33] Scuseria, G. E.; Janssen, C. L.; Schaefer, H. F. An efficient reformulation of the closed-shell coupled cluster single and double excitation (CCSD) equations. *J. Chem. Phys.* **1988**, *89*, 7382-7387.

[34] Raghavachari, K.; Trucks, G. W.; Pople, J. A.; Head-Gordon, M. Fifth-order perturbation comparison of electron correlation theories. *Chem. Phys. Lett.* **1989**, *157*, 479-483.

[35] Noga, J.; Bartlett, R. J. The full CCSDT model for molecular electronic structure. *J. Chem. Phys.* **1987**, *86*, 7041-7050; **1988**, *89*, 3041-3041.

[36] Scuseria, G. E.; Schaefer, H. F. A new implementation of the full CCSDT model for molecular electronic structure. *Chem. Phys. Lett.* **1988**, *152*, 382-386.

[37] Kendall, R. A.; Dunning, T. H.; Harriison, R. J. Electron affinities of the first-row atoms revisited. Systematic basis sets and wave functions. *J. Chem. Phys.* **1992**, *96*, 6796-6806.

[38] Woon, D.E.; Dunning, T. H. Gaussian basis sets for use in correlated molecular calculations. V. Core-valence basis sets for boron through neon. *J. Chem. Phys.* **1995**, *103*, 4572-4585.

[39] Prascher, B.; Woon, D. E.; Peterson, K. A.; Dunning, T. H.; Wilson, A. K. Gaussian basis sets for use in correlated molecular calculations. VII. Valence, core-valence, and scalar relativistic basis sets for Li, Be, Na, and Mg. *Theor. Chem. Acc.* **2011**, *128*, 69-82.

[40] Dunning, T. H. Gaussian basis sets for use in correlated molecular calculations I: the atoms boron through neon and hydrogen. *J. Chem. Phys.* **1989**, *90*, 1007-1023.

[41] Lim, I. S.; Schwerdtfeger, P.; Metz, B.; Stoll, H. All-electron and relativistic pseudopotential studies for the group 1 element polarizabilities from K to element 119. *J. Chem. Phys.* **2005**, *122*, 104103/1-12.

[42] Hill, J. G.; Peterson, K. A.; Gaussian basis sets for use in correlated molecular calculations. XI. Pseudopotential-based and all-electron relativistic basis sets for alkali metal (K-Fr) and alkaline earth (Ca-Ra) elements. *J. Chem. Phys.* **2017**, *147*, 244106/1-12.

[43] Stanton, J. F.; Gauss, J.; Harding, M. E.; Szalay, P. G. *CFOUR, a quantum chemical program package*, with contributions from Auer, A. A.; Bartlett, R. J.; Benedikt, U.; Berger, C.; Bernholdt, D. E.; Bomble, Y. J.; Cheng, L.; Christiansen, O.; Heckert, M.; Heun, O.; Huber, C.; Jagau, T.-C.; Jonsson, D.; Jusélius, J.; Klein, K.; Lauderdale, W. J.; Matthews, D. A.; Metzroth, T.; Mück, L. A.; O'Neill, D. P.; Price, D. R.; Prochnow, E.; Puzzarini, C.; Ruud, K.; Schiffmann, F.; Schwalbach, W.; Simmons, C.; Stopkowicz, S.; Tajti, A.; Vázquez, J.; Wang, F.; Watts, J. D. and the integral packages MOLECULE (Almlöf, J.; Taylor, P. R.), PROPS (Taylor, P.R.), ABACUS (Helgaker, T.; Jensen, H. J. Aa.; Jørgensen, P.; Olsen, J.), and ECP routines by Mitin, A. V.; van Wüllen., C. 2010. For the current version see http://www.cfour.de.

[44] Kállay, M.; Surján, P. R. Higher excitations in coupled-cluster theory. *J. Chem. Phys.* **2001**, *115*, 2945-2954.

[45] Veazey, S. E.; Gordy, W. Millimeter-wave molecular-beam spectroscopy: alkali fluorides. *Phys. Rev.* **1965**, *138*, A1303-A1311.

[46] Huber, K. P.; Herzberg, G. *Molecular Spectra and Molecular Structure. IV. Constants of Diatomic Molecules*, Van Nostrand Reinhold, 1979.

[47] Rezac, R.; Hobza, P. Ab initio quantum mechanical description of noncovalent interactions at its limits: approaching the experimental dissociation energy of the HF dimer. *J. Chem. Theory Comput.* **2014**, *10*, 3066-3073.

[48] Grabowski, S. J. Hydrogen bonding strength--measures based on geometric and topological parameters. *J. Phys. Org. Chem.* **2004**, *17*, 18-31.

[49] Hedderich, H. G.; Frum, C. I.; Engleman, R.; Bernath, P. F. The infrared emission spectra of LiF and HF. *Can. J. Chem.* **1991**, *69*, 1659-1671.

[50] Lovas, F. J.; Tiemann, E. Microwave spectral tables I. Diatomic molecules. *J. Phys. Chem. Ref. Data* **1974**, *3*, 609-769.

[51] Reed, A. E.; Weinstock, R. B.; Weinhold. F. Natural population analysis. *J. Chem. Phys.* **1985**, *83*, 735-746.

[52] Reed, A. E.; Curtiss, L. A.; Weinhold. F. Intermolecular Interactions from a natural bond orbital, donor-acceptor viewpoint. *Chem. Rev*. **1988**, *88*, 899-926.

[53] Glendening, E. D.; Landis, C. R.; Weinhold, F. Natural bond orbital methods. *WIRES Comput. Mol. Sci.* **2012**, *2*, 1-42.

[54] Glendening, E. D.; Badenhoop, J. K.; Reed, A. E.; Carpenter, J. E.; Bohmann, J. A.; Morales, C. M.; Landis, C. R.; Weinhold, F. *NBO 6.0.* Theoretical Chemistry Institute, University of Wisconsin, Madison, 2013. see http://nbo.chem.wisc.edu.

[55] Jeziorski, B.; Moszynski, R.; Szalewicz, K. Perturbation theory approach to intermolecular potential energy surfaces of van der Waals complexes. *Chem. Rev.* **1994**, *94*, 1887-1930.

[56] *MOLPRO, version 2010.1, a package of ab initio programs*, Werner, H.-J.; Knowles, P. J.; Knizia, G.; Manby, F. R.; Schütz, M.; Celani, P.; Korona, T.; Lindh, R.; Mitrushenkov, A.; Rauhut, G.; Shamasundar, K. R.; Adler, T. B.; Amos, R. D.; Bernhardsson, A.; Berning, A.; Cooper, D. L.; Deegan, M. J. O.; Dobbyn, A. J.; Eckert, F.; Goll, E.; Hampel, C.; Hesselmann, A.; Hetzer, G.; Hrenar, T.; Jansen, G.; Köppl, C.; Liu, Y.; Lloyd, A. W.; Mata, R. A.; May, A. J.; McNicholas, S. J; Meyer, W.; Mura, M. E.; Nicklaß, A.; O'Neill, D. P.; Palmieri, P.; Peng, D.; Pflüger, K.; Pitzer, R. M.; Reiher, M.; Shiozaki, T.; Stoll, H.; Stone, A. J.; Tarroni, R.; Thorsteinsson, T.; Wang, M.; Wolf, A. See http://www.molpro.net.

[57] Grabowski, S. J.; Alkorta, I.; Elguero, J. Complexes between dihydrogen and amine, phosphine, and arsine derivatives. Hydrogen bond versus pnictogen interaction. *J. Phys. Chem. A* **2013**, *117*, 3243-3251. (See Figure 1C)

Graphic TOC